NANO LETTERS

pubs.acs.org/NanoLett Letter

Laser Processing of Crumpled Porous Graphene/MXene Nanocomposites for a Standalone Gas Sensing System

Cheng Zhang,* Jinguo Chen, Jindong Gao, Guanglong Tan, Shaobo Bai, Kangwei Weng, Hua Min Chen, Xiaohong Ding,* Huanyu Cheng,* Yanhui Yang, and Jun Wang

Cite This: *Nano Lett.* 2023, 23, 3435−3443 Read Online

ACCESS | Metrics & More | Article Recommendations | Supporting Information

ABSTRACT: Integrating wearable gas sensors with energy harvesting and storage devices can create self-powered systems for continuous monitoring of gaseous molecules. However, the development is still limited by complex fabrication processes, poor stretchability, and sensitivity. Herein, we report the low-cost and scalable laser scribing of crumpled graphene/MXenes nanocomposite foams to combine stretchable self-charging power units with gas sensors for a fully integrated standalone gas sensing system. The crumpled nanocomposite designed in island-bridge device architecture allows the integrated self-charging unit to efficiently harvest kinetic energy from body movements into stable power with adjustable voltage/current outputs. Meanwhile, given the stretchable gas sensor with a large response of ∼1% ppm^{-1} and an ultralow detection limit of ∼5 ppb to NO_2/NH_3, the integrated system provides real-time monitoring of the exhaled human breath and the local air quality. The innovations in materials and structural designs pave the way for the future development of wearable electronics.

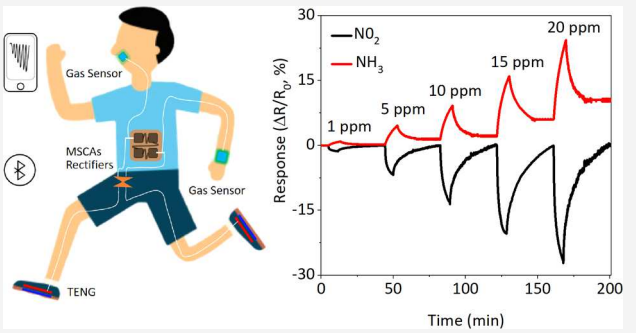

KEYWORDS: *crumpled porous graphene/MXene nanocomposites, triboelectric nanogenerator (TENG), microsupercapacitor arrays (MSCAs), standalone gas sensing system*

Practical applications of wearable sensors to detect and identify gas molecules for human health monitoring and improved quality of life hinge on the development of simple and cost-effective manufacturing methods, as well as miniaturization and system integration.[1,2] Although many recently reported wearable gas sensors exhibited remarkable sensitivity, low limit of detection, and flexibility, most of them are not fully stretchable and it is difficult to apply them on the skin with large mechanical deformations.[3] The challenges primarily come from the lack of highly sensitive and stable sensing devices under various forms of mechanical deformation and environmental variations, lightweight and deformable power supply modules with high energy storage performance, and effective methods to integrate the miniaturized systems.[4]

Wearable triboelectric nanogenerators (TENGs) can convert various types of renewable energy sources (e.g., mechanical motion, wind, etc.) into electricity.[5] However, the intermittent and alternating current (AC) output and mismatched current/voltage outputs from TENGs cannot be directly used to power most electronic devices. As a solution, wearable TENGs have been integrated with power management circuits and energy storage devices to provide self-powered charging units for practical use.[6] Furthermore, structural engineering of rigid materials and devices provides integrated wearable electronics with tissue-like mechanical properties and seamless contact with the hierarchically textured human skin. However, large-area fabrication of wearable electronics often suffers from expensive, complicated, and less reproducible manufacturing.

This article reports a low-cost, scalable laser scribing approach to fabricate a fully integrated standalone gas sensing system based on laser-induced graphene/MXene nanocomposites for real-time monitoring of the exhaled breath of the human subject and local air quality throughout the day. The long-term operation of the device platform is provided by a self-charging power unit consisting of the TENG, power management circuit, and microsupercapacitor arrays (MSCAs). Meanwhile, the stretchable gas sensor exhibits a large response of 1.36%/0.92% ppm^{-1}, an ultralow detection limit of 3/5 ppb, and a fast response/recovery to NO_2/NH_3. The wireless, real-time, and continuous monitoring of the exhaled breath of the human subject and air quality from the stretchable gas sensor directly driven by the integrated self-

Received: February 7, 2023
Revised: March 31, 2023
Published: April 4, 2023

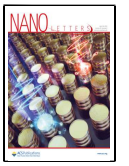

https://doi.org/10.1021/acs.nanolett.3c00454
Nano Lett. 2023, 23, 3435−3443

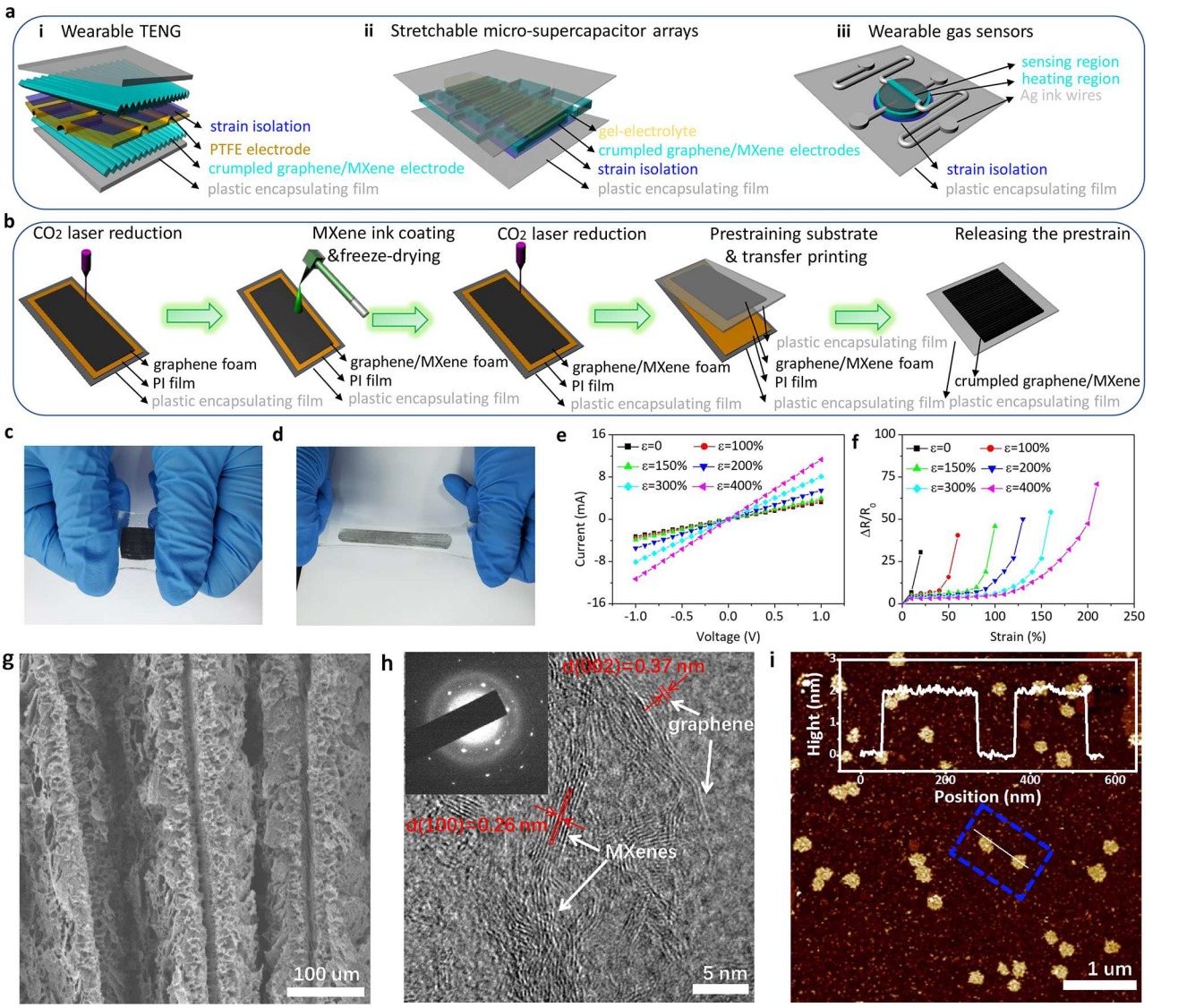

Figure 1. Standalone stretchable gas sensing system based on the crumpled porous graphene/MXene nanocomposite. (a) Schematic showing the (i) stretchable triboelectric nanogenerator (TENG), (ii) microsupercapacitor arrays (MSCAs), and (iii) gas sensor in the integrated system that is fabricated with (b) a two-step laser direct writing process with a prestrain strategy. Photographs of crumpled nanocomposite foam (c) before and (d) after stretching of 300% for ε_{pre} of 400%. (e) Linear current−voltage (I−V) curves and (f) the electromechanical response of the crumpled nanocomposite for different ε_{pre}: 0, 100, 150, 200, 300, and 400%. (g) Scanning electron microscopy (SEM) image and (h) high-resolution transmission electron microscopy (HRTEM) of the graphene/MXene foam. (i) Atomic force microscopy (AFM) image and height information on MXene nanosheets.

charging power unit provides the system-level proof-of-concept demonstration. The demonstrated design principles, materials selection, fabrication approaches, and system integration methods provide a complete toolkit to create the next-generation standalone stretchable electronics.

DEVICE DESIGN AND MATERIAL STRATEGY FOR THE STANDALONE GAS SENSING SYSTEM

The standalone stretchable gas sensing system is fabricated from laser direct writing of crumpled porous graphene/MXenes nanocomposite foams on a flexible elastomer substrate (Figure 1), allowing for conformal contact with the human skin (or textiles). In the self-powered charging unit, the wearable TENG assembled in shoes first generates sustained electrical energy from human motion. With a rectification circuit, the harvested intermittent and AC energy is stored in an all-in-one stretchable MSCAs with supercapacitor cells connected in series and/or in parallel to generate desirable current/voltage outputs to stably drive the gas sensing system.

The crumpled porous graphene/MXenes nanocomposite is chosen as the active material for all device components (i.e., TENG/MSCAs electrodes and gas sensor, Figure 1a). The nanocomposite is synthesized by a facile two-step direct laser writing process (Figure 1b). In brief, after spray coating MXenes on the 3D graphene foam prepared by a CO_2 laser under ambient conditions, a second laser scribing under the protection of argon generates the nanocomposite. Next, the crumpled nanocomposite is fabricated with a prestrain strategy as described in our previous work,[7,8] presenting a cost-effective strategy to introduce surface structures that can be well controlled by the prestrain level. The prestrain $\varepsilon_{pre} = (L - L_0)/L_0 \times 100\%$ is related to the original L_0 and stretched L length of the substrate. The crumpled porous structure provides the

https://doi.org/10.1021/acs.nanolett.3c00454
Nano Lett. 2023, 23, 3435−3443

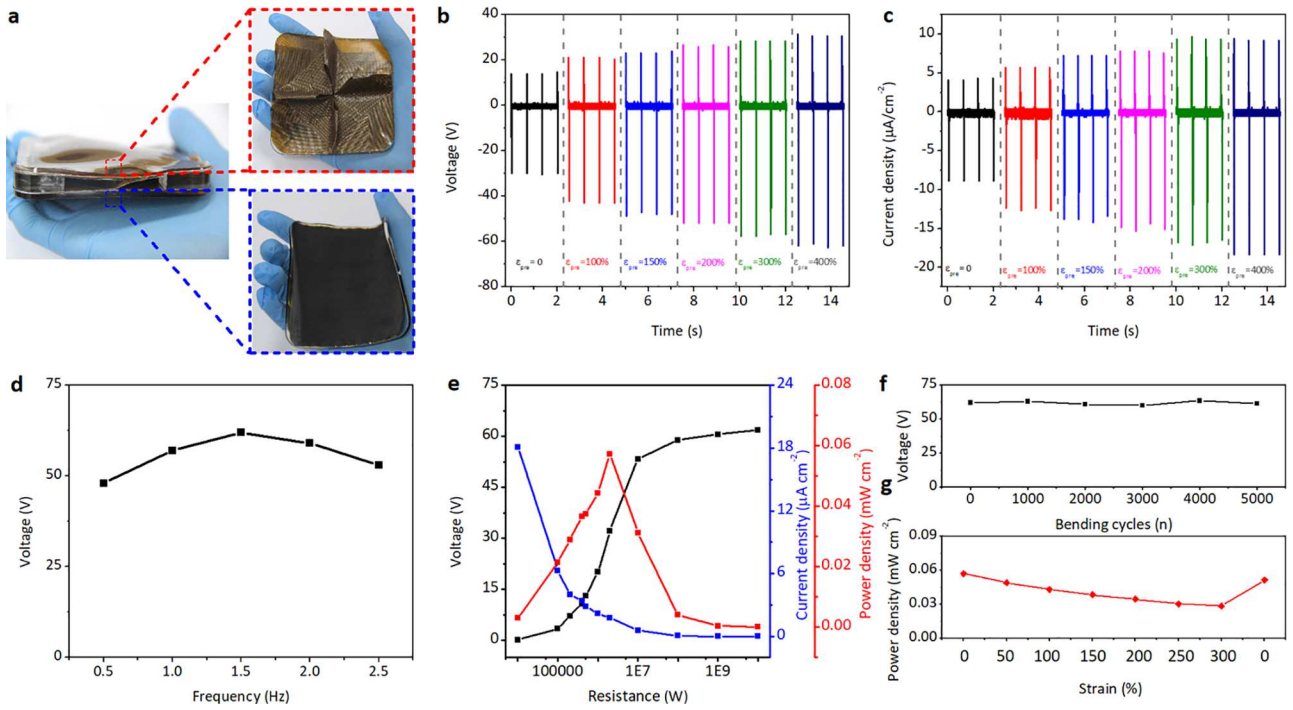

Figure 2. Performance of the stretchable graphene/MXene-based TENG. (a) Photograph of the stretchable TENG consisting of a top PTFE electrode with a kirigami layout and a bottom crumpled nanocomposite electrode (dimension of the TENG: 8.0 cm × 8.0 cm). Output (b) voltage and (c) current of the TENG as the prestrain level increases from 0 to 400% at a frequency of 1.5 Hz. (d) The output voltage of the TENG as a function of the frequency from 0.5 to 2.5 Hz for a prestrain of 400%. (e) Dependence of the output voltage, current density, and power density of TENG on the load resistance. (f) Output voltage as a function of bending cycles. (g) Changes in the peak output power density with the applied tensile strains.

resulting nanocomposite foam with high stretchability (Figure 1c, d). While the use of the waterproof PDMS presents a challenge to achieve high water transport capacity, it can be replaced by the sugar-templated PDMS[9] to effectively improve the breathability and level of comfort in the resulting device system. The electric conductivity of the crumpled graphene/MXenes increases with the increasing ε_{pre} (Figure 1e), due to the increased conductive pathways in the highly crumpled foams. The electromechanical performance of the crumpled graphene/MXenes is also enhanced to provide a higher stretchability as ε_{pre} increases (Figure 1f). The specific surface area of the crumpled graphene/MXenes also increases from 240 to 350 $m^2\ g^{-1}$ with the increasing ε_{pre} from 0 to 400% for improved the interfacial interactions between nanocomposites and charge carriers. The improved electrical conductivity, mechanical robustness, and specific surface area of the crumpled porous graphene/MXenes from the simple fabrication provide opportunities for applications in the standalone stretchable device platform.

Scanning electron microscopy image show crumpled structures in the porous nanocomposite (Figure 1g) to increase surface roughness and effective contact area for enhanced triboelectric charge densities, active sites for charge storage, and gas molecules adsorption.[10] The high-resolution transmission electron microscopy image identifies two interlayer distances of 0.37 and 0.26 nm corresponding to the (002) and (100) planes in graphitic materials and MXene (Figure 1h), respectively. The poly crystalline ring and hexagonal symmetry spot patterns of the selected area electron diffraction pattern also confirm wrinkled graphene layers and hexagonal structure of MXene. The smooth sheets in the atomic force microscopy exhibit a relatively uniform lateral size of ∼100 nm and an average thickness of 1.7 nm that corresponds to the height of a single-layered $Ti_3C_2T_x$ slab along the (002) direction (Figure 1i).[11] The more structural information on the as-prepared samples is investigated using Raman spectroscopy, X-ray diffraction, and X-ray photoelectron spectroscopy (Figures S1 and S2).

FABRICATION AND PERFORMANCE OF THE STRETCHABLE GRAPHENE/MXENE-BASED TENG

A PDMS layer is used as the spacer between the crumpled nanocomposite foam and kirigami polytetrafluoroethylene (PTFE) to control the gap distance in the stretchable TENG (Figure 2a). To comprehensively evaluate the TENG performance, the effects of vertical force, deformation frequency, and mechanical deformation are investigated by a linear mechanical motor (external force of 100 N). As the prestrain ε_{pre} increases from 0 to 100/150/200/300/400%, the output voltage increases from 30.5 V to 43.6/49.0/52.4/57.7/62.7 V for an external load resistance of 10 MΩ (Figure 2b), whereas the output current also increases from 8.9 to 18.4 $\mu A\ cm^{-2}$ by 106.7% (Figure 2c). As a result, ε_{pre} of 400% provides the best performance due to the highly rough surface and large effective contact area; thus, it is chosen in the following studies unless specified otherwise. As the deformation frequency increases from 0.5 to 2.5 Hz, the output voltage first increases and then decreases (Figure 2d). Increasing the load resistance in the range identifies the peak output power density of ca. 5.7×10^{-2} mW cm^{-2} at a resistance of 2 MΩ (Figure 2e). The output voltage of the TENG only decreases from 62.7 V to 61.5 by 1.9% as it is bent by 180° for 5000 cycles (Figure 2f). More importantly, as the tensile strain applied on the device

https://doi.org/10.1021/acs.nanolett.3c00454
Nano Lett. 2023, 23, 3435−3443

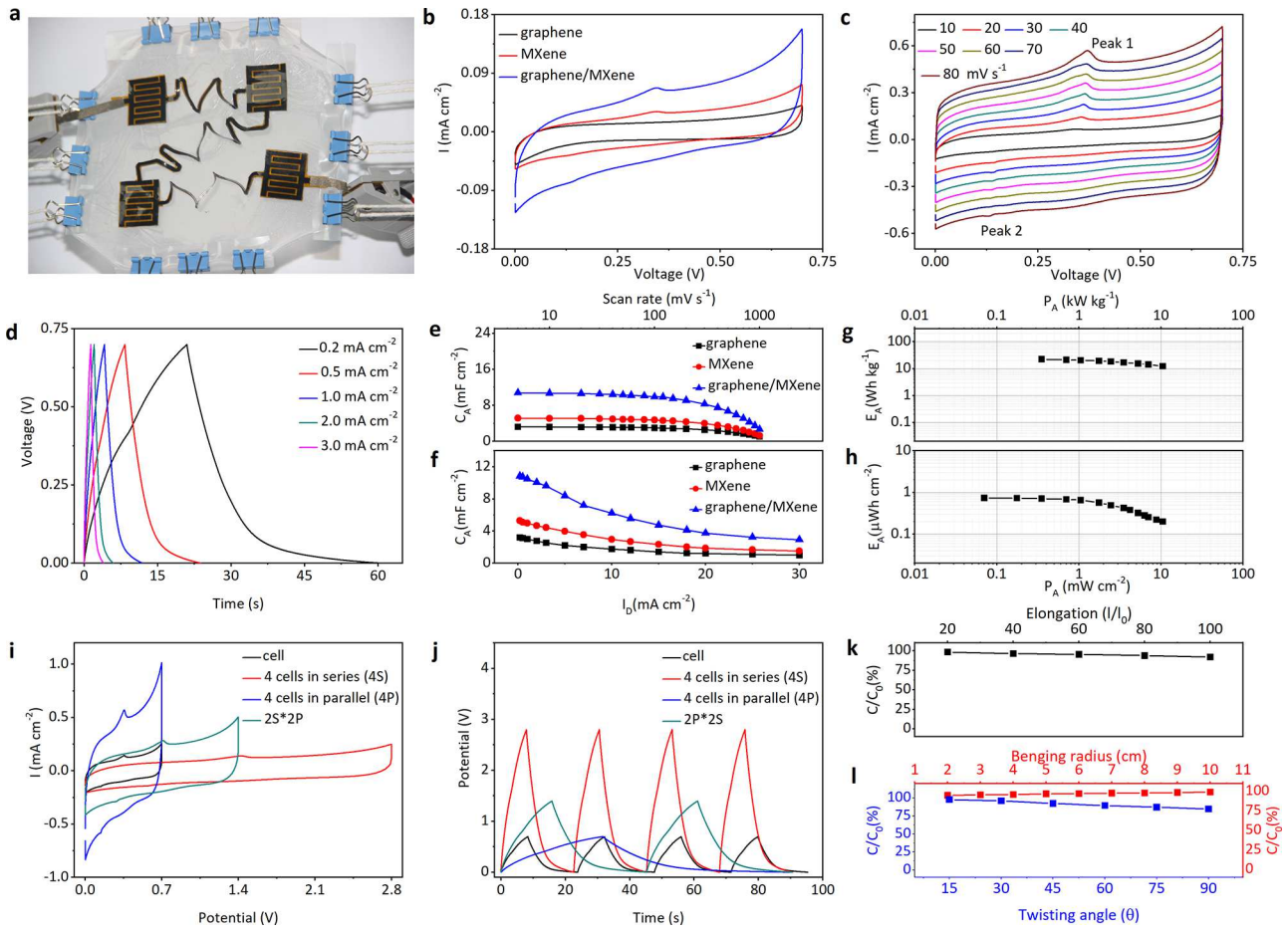

Figure 3. Performance characterization of the stretchable graphene/MXene-based MSCAs. (a) Photograph of stretchable MSCAs under 100% biaxial stretching. (b) Cyclic voltammetry (CV) curves of MSC cells based on porous graphene, MXene, and nanocomposite electrodes. (c) CV curves of the MSC cell based on nanocomposite electrodes (used in the following studies unless specified otherwise) at different scan rates from 10 to 80 mV s^{-1}. (d) Galvanostatic charge−discharge (GCD) plots at different current densities. The specific capacitance of MSC cell versus (e) scan rate and (f) discharge current density. (g, h) Ragone plots of our MSC cell. Real-time recorded (i) CV curves and (j) GCD plots of single devices and the all-in-one MSCAs with different serial and parallel connections. Capacitance retention of the all-in-one planar MSCAs after (k) stretching and (l) bending and twisting cycles.

increases from 0% to 300% (well beyond the stretching range on the skin surface), the output power density of the TENG gradually decreases from 5.7 × 10^{-2} to 2.9 × 10^{-2} mW cm^{-2} (Figure 2g). After the release of the strain, the output power density recovers to 5.2 × 10^{-2} mW cm^{-2}. The excellent output performance of the stretchable TENG compares favorably with those reported previously TENGs[12−15] (Table S1).

FABRICATION AND PERFORMANCE OF THE STRETCHABLE GRAPHENE/MXENE-BASED MSCAS

To continuously and stably provide sustained energy with specific output voltage/current, graphene/MXene-based MSCAs have been combined with TENGs to store the harvested intermittent energy. The integrated area under the cyclic voltammetry (CV) curve of the nanocomposite-based MSC is significantly larger than the as-prepared graphene- and MXene-based MSCs (Figure 3b). Furthermore, the shape of the CV and galvanostatic charge−discharge (GCD) curves is well maintained in the nanocomposite-based MSC at different scan rates and current densities (Figure 3c, d). The C_A of the composite-based MSC can achieve 10.8 mF cm^{-2} at 5 mV s^{-1}, which is ca. 2.1 and 3.3 times larger than that of MXene- and graphene-based MSCs (Figure 3e). Meanwhile, the nanocomposite-based MSC can deliver C_A of 10.9 mF cm^{-2} at 1 mA cm^{-2} and still maintain 2.9 mF cm^{-2} at 30 mA cm^{-2} (Figure 3f). Notably, the nanocomposite-based MSC can achieve an ultrahigh energy density of 22.46 Wh kg^{-1} (or 0.74 μWh cm^{-2}) at a power density of 0.35 kW kg^{-1} (or 0.07 mW cm^{-2}) (Figure 3g, h), which outperforms many previously reported all-in-solid MSC[16−20] (Table S2). In addition, the device shows a superior capacitance retention rate of 75% after 10 000 cycles at 2 mA cm^{-2}.

The high degree of adjustable electrical outputs is achieved by connecting multiple MSC cells with an island-bridge layout in series (S) and/or parallel (P). The serial configurations such as 2S and 2P*2S allow the output voltage to increase by 2 times, whereas the parallel configurations such as 2P and 2P*2S increase the current density by 2 times (Figure 3i). The excellent performance uniformity and scalability of the MSC devices are further confirmed by GCD curves at 0.5 mA cm^{-2} (Figure 3j).

Taken together with the strain isolation strategy, the MSCAs can be stretched 100% along the *x* and *y* directions (Figure 3a). The capacitance retention can achieve 92% even at a tensile strain of 100% (Figure 3k). After 100 cycles of bending at a radius of 10/9/8/7/6/5/4/3/2 cm, the capacitance

https://doi.org/10.1021/acs.nanolett.3c00454
Nano Lett. 2023, 23, 3435−3443

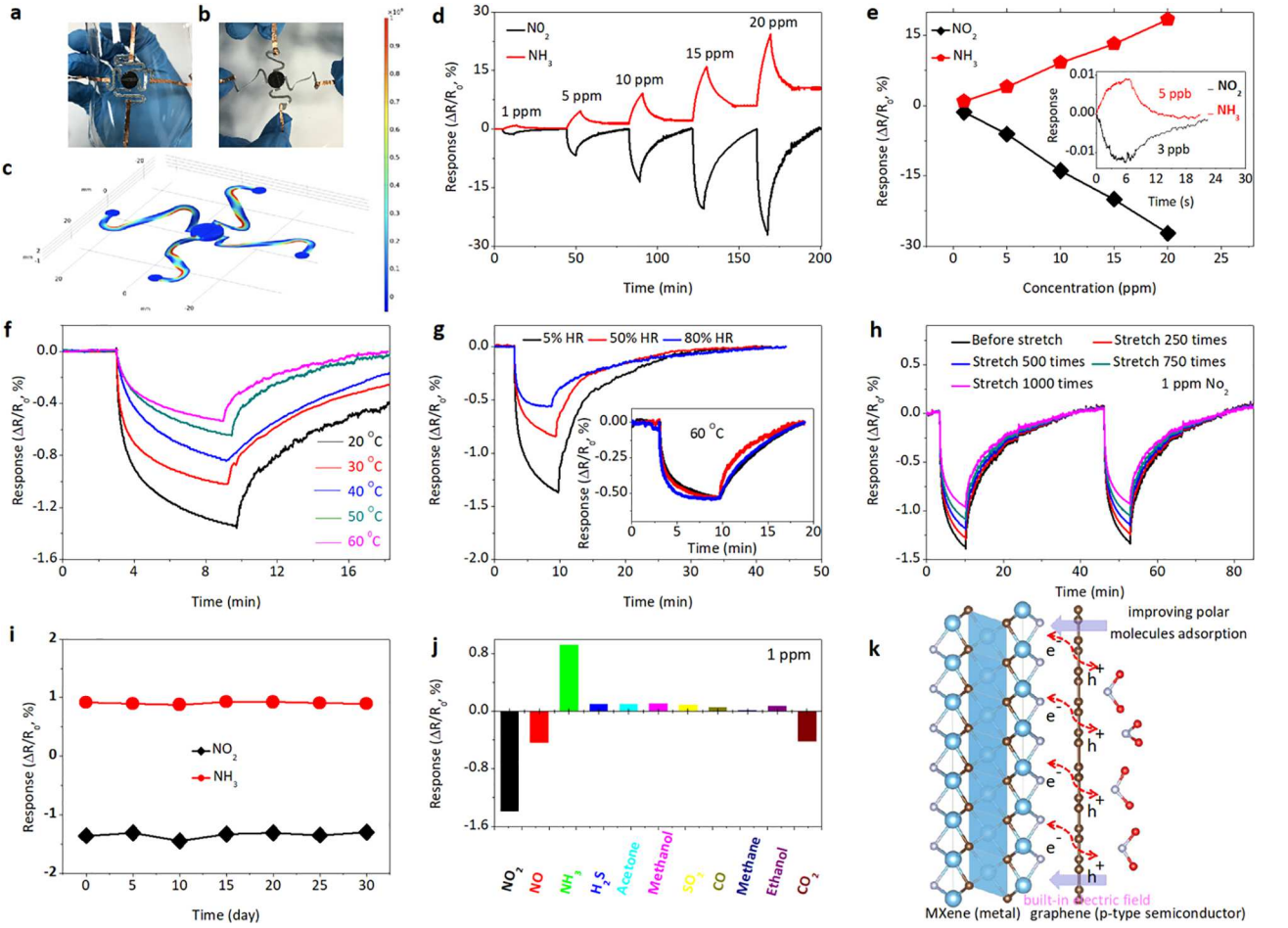

Figure 4. Performance evaluation of the graphene/MXene nanocomposite-based gas sensors. Photographs of the stretchable gas sensors under (a) bending radius of 1 cm and (b) 100% stretching. (c) Strain distribution in the gas sensor under 100% stretching. (d) Real-time sensing response of graphene/MXene nanocomposite-based gas sensors to NO_2/NH_3 from 1 to 20 ppm and (e) its calibration curve, with the sensor response to 3/5 ppb NO_2/NH_3 shown in the inset. Sensor responses to 1 ppm of NO_2 at (f) various temperatures from self-heating and (g) different relative humidity (RH) levels at room temperature, with the result at 60 °C from self-heating shown in the inset. (h) The real-time sensing curves of the stretchable gas sensor to 1 ppm of NO_2 before and after 250/500/750/1000 cyclic stretching/releasing cycles (a uniaxial tensile strain of 25%). (i) Long-term stability of the sensor over a month (1 ppm of NO_2/NH_3). (j) The selectivity of the stretchable gas sensor. (k) Schematic showing the adsorption/desorption of gas molecules.

retention rates remain over 99.2/98.7/98.3/97.5/96.9/96.3/95.8/95% respectively (Figure 3l). The cycling performance also shows negligible capacitance degrading after 100 twisting cycles at a twist angle of 90° (Figure 3l).

ENVIRONMENTAL AND MECHANICAL STABILITY OF THE STRETCHABLE GRAPHENE/MXENE-BASED SENSORS

The gas sensor consists of a front sensing region and a back heating region both based on graphene/MXene configured in the islands-bridge layout. The graphene/MXene-based gas sensors are highly flexible and stretchable (Figure 4a, b), allowing seamless integration and conformal contact with textured human skin. The peak principal strain in the active gas sensors is only 1.2% for an applied tensile strain of 100%, due to the unfolding of the serpentine interconnections as revealed by the finite element analysis (FEA) (Figure 4c). The combination of strain isolation and island-bridge design helps reduce the strain effect during gas detection. In addition, other decoupling sensing strategies[21] can be used to further minimize the strain effect for improved gas sensing accuracy in the presence of complex mechanical deformations.

Characterization of the gas-sensing performance to the target concentration of gas (e.g., NO_2 and NH_3) is performed in a dynamic gas distribution instrument at room temperature (20 °C), providing the response as $\Delta R/R_0 = (R - R_0)/R_0$, where R_0 and R are the resistances of the gas sensor in the synthetic air and target gas. As the gas concentration of NO_2 (or NH_3) is increased from 1 to 20 ppm, the conductance of the graphene/MXene-based gas sensor increases (or decreases) (Figure 4d). Furthermore, the response magnitude decreases (or increases) almost linearly with increased NO_2 (or NH_3) concentrations (Figure 4e), with ultrahigh sensitivity of 1.51 (or 0.98) ppm^{-1}. The sensor also exhibits an ultrahigh signal-to-noise ratio (SNR) of 225 (or 122) to 100 ppb NO_2 (or NH_3), leading to an estimated limit of detection (LOD) of 1.2 (or 2.3) ppb to NO_2 (or NH_3) (at SNR of 3). It is worth noting that the SNR of our sensor can still achieve 2.7 (or 2.8) for 3 ppb NO_2 (or 5 ppb NH_3) (Figure 4e, inset), which compares favorably over previously reported NO_2/NH_3 gas sensors (Table S3).

https://doi.org/10.1021/acs.nanolett.3c00454
Nano Lett. 2023, 23, 3435−3443

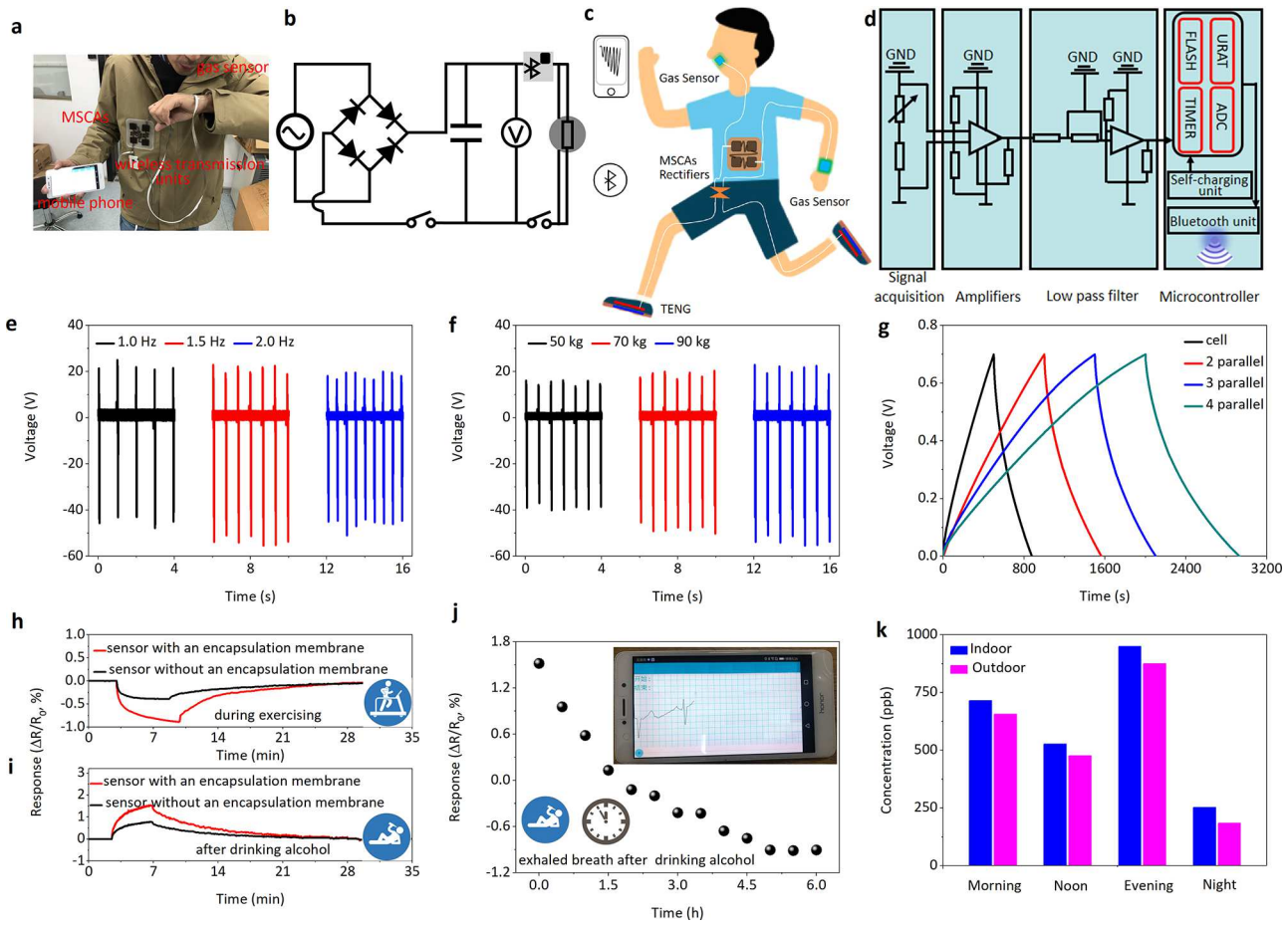

Figure 5. Demonstration of the standalone stretchable nanocomposite-based gas sensing platform for environmental monitoring. (a) Photograph, (b) circuit diagram, and (c) schematic of the integrated standalone platform on the fabrics on the human subject. (d) The circuit design of the wireless transmission module. The output voltage of the stretchable TENG (e) at varying driving frequencies from (f) human subjects of different body weights. (g) The voltage of the stretchable MSCAs with different numbers of MSCs connected in parallel charged by the TENG (from a human subject of 90 kg at 1.5 Hz, discharge at 5 μA). Responses of the integrated standalone sensing platform with/without an encapsulation membrane to the exhaled breath of the human subject (h) during exercising and (i) after drinking alcohol. (j) The real-time monitoring of the exhaled breath of the human subject after drinking alcohol. (k) Applications of the standalone gas sensing platform for monitoring indoor and outdoor NO_2 from car exhaust at different times of the day powered by self-charging units.

Joule heating of the back heating region is explored to modulate the gas sensing performance. As the applied voltage during the resistance measurement is increased from 0.7 to 2.8 V with a step size of 0.7 V, the stable temperature starts in the sensor can reach from 30 to 60 °C with a step size of 10 °C (Figure S6). The increased temperature results in decreased response/recovery time from ~7/32 min to 6/19 min, as well as a reduced response from 1.36% to 0.54% (to 1 ppm of NO_2) (Figure 4f). As both graphene and MXene are sensitive to humidity, adsorption competition occurs between gas and water molecules. As a result, the gas sensor exhibits a decreased response from 1.31% to 0.57% (to 1 ppm of NO_2) when the relative humidity (RH) level is increased from 5% to 80% at room temperature (Figure 4g). Although the gas sensor with a waterproof but gas-permeable PDMS membrane can reduce the impact of the RH on the sensing performance, it cannot remove the water molecules adsorbed on the sensor surface in extremely high RH levels or over time.[22] However, this challenge can be effectively addressed by operating the gas sensor at elevated temperatures from self-heating due to the generated thermal radiation. There is no appreciable degradation in the sensor response under various RH levels at 60 °C (Figure 4g inset).

Although the resistance of the nanocomposite electrode slightly increases with the increasing applied tensile strain (Figure S7), the response of the gas sensor to 1 ppm of NO_2 can still reach 1.34/1.32/1.26/1.15% (with a retention of 98.5/97.1/92.6/84.6%) at a uniaxial tensile strain of 25/50/75/100%. Despite a small degradation after 1000 stretching and releasing cycles of 25%, the response/recovery to 1 ppm of NO_2 at room temperature is well-maintained, with a response of 1.16% (Figure 4h). The sensor also shows reliable long-term stability, with 95/93% of the initial value to 1 ppm of NO_2/NH_3 after a month (Figure 4i). Furthermore, the sensor responses NO_2/NH_3 (−1.36%/0.92%) are much larger than those to NO, H_2S, acetone, methanol, SO_2, CO, methane, ethanol, and CO_2, demonstrating excellent selectivity for NO_2 and NH_3 gas (Figure 4j).

The high sensitivity of the graphene/MXene-based sensor results from the free electrons transfer from *p*-type laser-induced graphene to the metallic $Ti_3C_2T_x$ MXene at the interface until the Fermi levels of the two are aligned, due to the work function difference (5.28 eV for MXene and 4.7 eV

https://doi.org/10.1021/acs.nanolett.3c00454
Nano Lett. 2023, 23, 3435−3443

for graphene in air).[23] At equilibrium, a Helmholtz double layer and a built-in electric field are established at the nanohybrid interface (Figure S8), with negatively charged MXene and positively charged graphene near its surface.[24] This charge separation in nanohybrids provides (1) an increased number of holes in the laser-induced graphene for increased electrical conductivity, and (2) the built-in electric field at the interface to induce further electrical polarization of the nanohybrids (a driving force for gas sensing without the external bias voltage) (Figure 4k).[25]

STANDALONE STRETCHABLE GAS SENSING PLATFORM FOR ENVIRONMENTAL MONITORING

The self-powered charging units as a sustained power source can drive gas sensors and wireless communication units with Bluetooth chips (CC2541) for sending data to the user interface (Figure 5a–d). The TENG generates a maximum output voltage of 48.4/55.2/51.8 V as the volunteer running with a body weight of 50 kg runs at a frequency of 1.0/1.5/2.0 Hz (Figure 5e). At a constant frequency of 1.5 Hz, the human subject with increasing body weight from 50 to 70 and then to 90 kg provides an increased output voltage from 55.2 to 69.5 and then 76.2 V (Figure 5f). The stretchable MSCAs charged by the insole TENG exhibits a steady increase in the voltage to reach the operating voltage, indicating successful storage of the harvested energy (Figure 5g). In addition, the slow decrease of the voltage in the GCD tests at 5 μA indicates the stable output of the self-charging power unit. Specifically, it takes 498.2/1001.1/1493.3/1996.2 s to charge and then 382.5/559.2/612.6/936.7 s to discharge the 1S*1P/2P/3P/4P MSCAs. However, the peak output power density is reduced to 1.6×10^{-2} mW cm^{-2} when the insole TENG is driven by walking of a human subject with a body weight of 90 kg at 1 Hz and the operating voltage of the MSC is decreased to 0.4 V charged by the TENG (Figure S11). The reduced performance is likely attributed to the self-discharge process resulting from the intermittent charging process. Therefore, further improvements in the power outputs of TENG and electrochemical performances of MSC are highly desirable to sustainably operate the fully integrated standalone gas sensing system for long-term operation during walking. These results show the favorable integration and adjustable power outputs of the nanocomposite-based self-charging power unit.

As a proof-of-concept demonstration, the on-skin standalone stretchable gas sensing platform driven by human motion during vigorous exercises provides a viable means to continuously monitor the exhaled breath of the human subject and NO_2 from car exhaust. In order to avoid the direct impact of the airflow on the stability and accuracy of the sensor, the exhaled human breath is first collected by a PET face mask and then introduced to the gas bottle with the sensor mounted inside using a PET pipe (Figure S12). The standalone gas sensing platform with and without a waterproof but gas-permeable PDMS membrane allows continuous breath analysis of the human subject during varying activities.[26] By eliminating the influence of moisture and relative humidity variations, the on-skin standalone stretchable gas sensing platform with the semipermeable PDMS membrane provides a more accurate measurement of gas components in human breath (Figure 5h, i). The continuous analysis of the breath from the human subject after drinking alcohol provides a simple yet viable means to evaluate the influence of alcohol (Figure 5j). The measured peak ethanol concentration of 1600 ppb from a human subject after drinking 200 mL of alcohol (2 h to recover) agrees reasonably well with the value of 1400 ppb measured by a commercial alcohol sensor (MQ3, 2.5 h to recover) (Figure S13). Furthermore, the stretchable gas sensor is powered to wirelessly and continuously monitor NO_2 gas from car exhaust in the morning, noon, evening, and night. By assuming NO_2 as the major active gas molecule, the measured response from our platform of −1.064/−0.841/−1.340/−0.513% in the morning/noon/evening/night corresponds to the concentration of NO_2 of 715/527/950/252 ppb (Figure 5k). The results are almost consistent with those measured by the commercial NO_2 gas sensor (XENSIV PAS, Figure S14). Furthermore, the cycling stability of the standalone gas sensing platform is evaluated by repeated sensing cycles to 1 ppm of NO_2 at room temperature for 50 days (Figure S15). The gas response and response/recovery rates remain nearly stable, indicating the long-term stability of the standalone gas sensing platform for real-life applications.

In summary, laser processing of crumpled porous graphene/MXene nanocomposites has been developed for a standalone gas sensing system by integrating stretchable TENG with MSCAs and a gas sensor configured in the island-bridge layout. The crumpled porous graphene/MXene nanocomposite provides large effective triboelectric areas in TENGs, introduces more electrochemically active sites for electro-ionic charge storage in MSCAs, and increases the gas molecule adsorption site and charge transfer process for gas sensing. Besides the nanocomposite materials with excellent performance parameters, the highly stretchable devices with modulated output performance by the island-bridge and self-heating designs offer benefits for easy device fabrication and future scaling up. The resulting integrated standalone stretchable device platform allows self-powered and continuous monitoring of the human conditions in the exposed local environment under complex mechanical deformations on human skin or clothing. The design strategies and demonstrations from this work pave the way for the design, fabrication, and application of the next-generation biointegrated electronics for healthy aging and precision medicine.

ASSOCIATED CONTENT

Supporting Information

The Supporting Information is available free of charge at https://pubs.acs.org/doi/10.1021/acs.nanolett.3c00454.

Experimental section; SEM, TEM, AFM, Raman, XRD, XPS of graphene, MXene, and crumpled porous graphene/MXene nanocomposite; schematic to show the working principle of the crumpled porous graphene/MXene-based TENG under cyclic compressive force; electrochemical characterization of an all-in-one planar MSC device; real-time sensing responses of sensors based on 3D porous graphene/MXene foam and compressed graphene/MXene film; temperature curves of the sensor; resistance and response of the stretchable gas sensor; energy band diagrams of graphene/MXene nanocomposite; density functional theory (DFT) simulations; performance of the as-prepared stretchable graphene/MXene-based TENG driven by human motion; comparison between the actual NO_2 concentrations in the outdoor and the response from the as-prepared wearable gas sensor; cycling stability of the

https://doi.org/10.1021/acs.nanolett.3c00454
Nano Lett. 2023, 23, 3435−3443

standalone stretchable nanocomposite-based gas sensing platform (PDF)

AUTHOR INFORMATION

Corresponding Authors

Cheng Zhang − *Fujian Key Laboratory of Functional Marine Sensing Materials, College of Material and Chemical Engineering, Minjiang University, Fuzhou 350108, PR China; Department of Engineering Science and Mechanics, Materials Research Institute, Pennsylvania State University, University Park, Pennsylvania 16802, United States;* orcid.org/0000-0001-5810-9680; Email: zhangcheng@mju.edu.cn

Xiaohong Ding − *Fujian Provincial Key Laboratory of Eco-Industrial Green Technology, College of Ecological and Resources Engineering, Wuyi University, Wuyishan 354300, PR China; Department of Engineering Science and Mechanics, Materials Research Institute, Pennsylvania State University, University Park, Pennsylvania 16802, United States;* orcid.org/0000-0002-9693-2691; Email: dxh@wuyiu.edu.cn

Huanyu Cheng − *Department of Engineering Science and Mechanics, Materials Research Institute, Pennsylvania State University, University Park, Pennsylvania 16802, United States;* orcid.org/0000-0001-6075-4208; Email: huanyu.cheng@psu.edu

Authors

Jinguo Chen − *Fujian Key Laboratory of Functional Marine Sensing Materials, College of Material and Chemical Engineering, Minjiang University, Fuzhou 350108, PR China*

Jindong Gao − *Fujian Key Laboratory of Functional Marine Sensing Materials, College of Material and Chemical Engineering, Minjiang University, Fuzhou 350108, PR China*

Guanglong Tan − *Fujian Key Laboratory of Functional Marine Sensing Materials, College of Material and Chemical Engineering, Minjiang University, Fuzhou 350108, PR China*

Shaobo Bai − *Fujian Key Laboratory of Functional Marine Sensing Materials, College of Material and Chemical Engineering, Minjiang University, Fuzhou 350108, PR China*

Kangwei Weng − *Fujian Key Laboratory of Functional Marine Sensing Materials, College of Material and Chemical Engineering, Minjiang University, Fuzhou 350108, PR China*

Hua Min Chen − *Fujian Key Laboratory of Functional Marine Sensing Materials, College of Material and Chemical Engineering, Minjiang University, Fuzhou 350108, PR China*

Yanhui Yang − *Fujian Key Laboratory of Functional Marine Sensing Materials, College of Material and Chemical Engineering, Minjiang University, Fuzhou 350108, PR China*

Jun Wang − *Fujian Key Laboratory of Functional Marine Sensing Materials, College of Material and Chemical Engineering, Minjiang University, Fuzhou 350108, PR China*

Complete contact information is available at: https://pubs.acs.org/10.1021/acs.nanolett.3c00454

Author Contributions

Cheng Zhang and Huanyu Cheng: Conceptualization, Investigation, Writing - review and editing. **Jinguo Chen, Jindong Gao, Guanglong tan, Huamin Chen Xiaohong Ding, Yanhui Yang,** and **Jun Wang:** Investigation, Data Curation.

Notes

The authors declare no competing financial interest.

ACKNOWLEDGMENTS

This work is supported by the National Natural Science Foundation of China (No. 52002162, 12174172), the Natural Science Foundation of Fujian (No. 2021J011040, 2021J05249), the Fuzhou science and technology project (2021-SG-273). H.C. acknowledges the support provided by NIH (Award Nos. R21EB030140, U01DA056242, and R61HL154215), NSF (Grant Nos. ECCS-1933072 and 2222654), and Penn State University.

REFERENCES

(1) Kalantar-Zadeh, K.; Berean, K. J.; Ha, N.; Chrimes, A. F.; Xu, K.; Grando, D.; Ou, J. Z.; Pillai, N.; Campbell, J. L.; Brkljača, R.; Taylor, K. M.; Burgell, R. E.; Yao, C. K.; Ward, S. A.; McSweeney, C. S.; Muir, J. G.; Gibson, P. R. A human pilot trial of ingestible electronic capsules capable of sensing different gases in the gut. *Nat. Electron.* **2018**, *1* (1), 79−87.

(2) Schedin, F.; Geim, A. K.; Morozov, S. V.; Hill, E. W.; Blake, P.; Katsnelson, M. I.; Novoselov, K. S. Detection of individual gas molecules adsorbed on graphene. *Nat. Mater.* **2007**, *6* (9), 652−655.

(3) Lin, Y.; Chen, J.; Tavakoli, M. M.; Gao, Y.; Zhu, Y.; Zhang, D.; Kam, M.; He, Z.; Fan, Z. Printable Fabrication of a Fully Integrated and Self-Powered Sensor System on Plastic Substrates. *Adv. Mater.* **2019**, *31* (5), 1804285.

(4) Yang, Y.; Song, Y.; Bo, X.; Min, J.; Pak, O. S.; Zhu, L.; Wang, M.; Tu, J.; Kogan, A.; Zhang, H.; Hsiai, T. K.; Li, Z.; Gao, W. A laser-engraved wearable sensor for sensitive detection of uric acid and tyrosine in sweat. *Nat. Biotechnol.* **2020**, *38* (2), 217−224.

(5) Wang, Z. L.; Song, J. Piezoelectric Nanogenerators Based on Zinc Oxide Nanowire Arrays. *Science* **2006**, *312* (5771), 242−246.

(6) Wang, Z. L.; Wu, W. Nanotechnology-Enabled Energy Harvesting for Self-Powered Micro-/Nanosystems. *Angew. Chem., Int. Ed.* **2012**, *51* (47), 11700−11721.

(7) Zhang, C.; Peng, Z.; Huang, C.; Zhang, B.; Xing, C.; Chen, H.; Cheng, H.; Wang, J.; Tang, S. High-energy all-in-one stretchable micro-supercapacitor arrays based on 3D laser-induced graphene foams decorated with mesoporous ZnP nanosheets for self-powered stretchable systems. *Nano Energy* **2021**, *81*, 105609.

(8) Zhang, C.; Chen, H.; Ding, X.; Lorestani, F.; Huang, C.; Zhang, B.; Zheng, B.; Wang, J.; Cheng, H.; Xu, Y. Human motion-driven self-powered stretchable sensing platform based on laser-induced graphene foams. *Appl. Phys. Rev.* **2022**, *9* (2), 029901.

(9) Yang, X.-Y.; Chen, L.-H.; Li, Y.; Rooke, J. C.; Sanchez, C.; Su, B.-L. Hierarchically porous materials: synthesis strategies and structure design. *Chem. Soc. Rev.* **2017**, *46* (2), 481−558.

(10) Zheng, B.; Zhao, G.; Yan, Z.; Xie, Y.; Lin, J. Direct Freeform Laser Fabrication of 3D Conformable Electronics. *Adv. Funct. Mater.* **2023**, *33* (1), 2210084.

(11) Naguib, M.; Mochalin, V. N.; Barsoum, M. W.; Gogotsi, Y. 25th Anniversary Article: MXenes: A New Family of Two-Dimensional Materials. *Adv. Mater.* **2014**, *26* (7), 992−1005.

(12) Chen, H.; Bai, L.; Li, T.; Zhao, C.; Zhang, J.; Zhang, N.; Song, G.; Gan, Q.; Xu, Y. Wearable and robust triboelectric nanogenerator based on crumpled gold films. *Nano Energy* **2018**, *46*, 73−80.

(13) Pu, X.; Liu, M.; Chen, X.; Sun, J.; Du, C.; Zhang, Y.; Zhai, J.; Hu, W.; Wang, Z. L. Ultrastretchable, transparent triboelectric nanogenerator as electronic skin for biomechanical energy harvesting and tactile sensing. *Sci. Adv.* **2017**, *3* (5), No. e1700015.

(14) Dong, K.; Wang, Y.-C.; Deng, J.; Dai, Y.; Zhang, S. L.; Zou, H.; Gu, B.; Sun, B.; Wang, Z. L. A Highly Stretchable and Washable All-Yarn-Based Self-Charging Knitting Power Textile Composed of Fiber Triboelectric Nanogenerators and Supercapacitors. *ACS Nano* **2017**, *11* (9), 9490−9499.

(15) Zou, Y.; Tan, P.; Shi, B.; Ouyang, H.; Jiang, D.; Liu, Z.; Li, H.; Yu, M.; Wang, C.; Qu, X. A bionic stretchable nanogenerator for underwater sensing and energy harvesting. *Nat. Commun.* **2019**, *10* (1), 2695.
(16) Lin, J.; Peng, Z.; Liu, Y.; Ruiz-Zepeda, F.; Ye, R.; Samuel, E. L. G.; Yacaman, M. J.; Yakobson, B. I.; Tour, J. M. Laser-induced porous graphene films from commercial polymers. *Nat. Commun.* **2014**, *5* (1), 5714.
(17) Yan, J.; Ren, C. E.; Maleski, K.; Hatter, C. B.; Anasori, B.; Urbankowski, P.; Sarycheva, A.; Gogotsi, Y. Flexible MXene/Graphene Films for Ultrafast Supercapacitors with Outstanding Volumetric Capacitance. *Adv. Funct. Mater.* **2017**, *27* (30), 1701264.
(18) Zhou, C.; Zhang, Y.; Li, Y.; Liu, J. Construction of High-Capacitance 3D CoO@Polypyrrole Nanowire Array Electrode for Aqueous Asymmetric Supercapacitor. *Nano Lett.* **2013**, *13* (5), 2078−2085.
(19) He, Y.; Chen, W.; Li, X.; Zhang, Z.; Fu, J.; Zhao, C.; Xie, E. Freestanding Three-Dimensional Graphene/MnO_2 Composite Networks As Ultralight and Flexible Supercapacitor Electrodes. *ACS Nano* **2013**, *7* (1), 174−182.
(20) Bae, J.; Song, M. K.; Park, Y. J.; Kim, J. M.; Liu, M.; Wang, Z. L. Fiber Supercapacitors Made of Nanowire-Fiber Hybrid Structures for Wearable/Flexible Energy Storage. *Angew. Chem., Int. Ed.* **2011**, *50* (7), 1683−1687.
(21) Yang, R.; Zhang, W.; Tiwari, N.; Yan, H.; Li, T.; Cheng, H. Multimodal Sensors with Decoupled Sensing Mechanisms. *Adv. Sci.* **2022**, *9* (26), 2202470.
(22) Yang, L.; Yi, N.; Zhu, J.; Cheng, Z.; Yin, X.; Zhang, X.; Zhu, H.; Cheng, H. Novel gas sensing platform based on a stretchable laser-induced graphene pattern with self-heating capabilities. *J. Mater. Chem. A* **2020**, *8* (14), 6487−6500.
(23) Mariano, M.; Mashtalir, O.; Antonio, F. Q.; Ryu, W.-H.; Deng, B.; Xia, F.; Gogotsi, Y.; Taylor, A. D. Solution-processed titanium carbide MXene films examined as highly transparent conductors. *Nanoscale* **2016**, *8* (36), 16371−16378.
(24) Zhang, Z.; Yates, J. T., Jr. Band Bending in Semiconductors: Chemical and Physical Consequences at Surfaces and Interfaces. *Chem. Rev.* **2012**, *112* (10), 5520−5551.
(25) Kim, Y.; Lee, S.; Song, J.-G.; Ko, K. Y.; Woo, W. J.; Lee, S. W.; Park, M.; Lee, H.; Lee, Z.; Choi, H.; Kim, W.-H.; Park, J.; Kim, H. 2D Transition Metal Dichalcogenide Heterostructures for p- and n-Type Photovoltaic Self-Powered Gas Sensor. *Adv. Funct. Mater.* **2020**, *30* (43), 2003360.
(26) Yang, L.; Zheng, G.; Cao, Y.; Meng, C.; Li, Y.; Ji, H.; Chen, X.; Niu, G.; Yan, J.; Xue, Y.; Cheng, H. Moisture-resistant, stretchable NO_x gas sensors based on laser-induced graphene for environmental monitoring and breath analysis. *Microsyst. Nanoeng.* **2022**, *8* (1), 78.

https://doi.org/10.1021/acs.nanolett.3c00454
Nano Lett. 2023, 23, 3435−3443